

# Xe Adsorption on a decagonal $\text{Al}_7\text{Ni}_{10}\text{C}_{017}$ quasicrystal surface

Wahyu Setyawan<sup>1</sup>, Nicola Ferralis<sup>2</sup>, Renee D. Diehl<sup>2</sup>, Milton W. Cole<sup>2</sup>, Stefano Curtarolo<sup>1,3</sup>

<sup>1</sup>Department of Mechanical Engineering and Materials Science, Duke University, Durham, NC 27708

<sup>2</sup>Department of Physics and Materials Research Institute, Penn State University, University Park, PA 16802

<sup>3</sup>corresponding author, e-mail: stefano@duke.edu

(May 24, 2021)

The grand canonical Monte Carlo method is employed to study the adsorption of Xe on a quasicrystalline  $\text{Al}_7\text{Ni}_{10}\text{C}_{017}$  surface. The calculation uses a semi-empirical gas-surface interaction, based on conventional combining rules and the usual Lennard-Jones Xe-Xe interaction. The resulting adsorption isotherms and calculated structures are consistent with the results of LEED experimental data. In this paper we focus on features not discussed earlier (Phys. Rev. Lett. 95, 136104 (2005)): the range of the average density of the adsorbate, the order of the transition, the orientational degeneracy of the ground state, the isosteric heat of adsorption of the system, and the effect of the vertical cell dimension.

## I. INTRODUCTION

The adsorption of simple gases on essentially flat surfaces has been studied extensively for the last 50 years, beginning with early experiments on exfoliated graphite [1,3]. Many phenomena that are found to occur in these systems are reasonably well described by the two-dimensional (2D) approximation [3]. However, this approximation fails to capture some of the more intriguing kinds of behavior, which make the subject of monolayer films diverse and challenging. A variety of monolayer phenomena can be attributed to competing adsorbate-adsorbate and adsorbate-substrate interactions; the relevant variables are the substrate symmetry and the interaction strengths and length scales of the adsorbate relative to those of the substrate [4,5].

Recently, our group has begun to explore the behavior of simple gases physisorbed on quasicrystalline surfaces [6,7]. The first system that we have explored extensively is Xe on the surface of the quasicrystal  $\text{d-Al}_7\text{Ni}_{10}\text{C}_{017}$  [8]. Ours is not the first study of film growth on quasicrystalline surfaces. A variety of growth modes has been seen in previous studies on a variety of substrates [9]. A key difference between our work and the previous investigations is that Xe is expected to be physically adsorbed, although we will see that the atomic binding energy lies near the upper limit of the regime normally ascribed to physical interactions (binding energy  $\approx 0.3$  eV). One advantage of physisorption relative to stronger binding adsorption is the presumption that the physisorption process does not alter the interacting partners significantly. That is, the surfaces do not reconstruct due to the film's presence and the adatoms retain their chemical identity, interacting with each other with forces similar to their gas phase interaction. A substantial body of experimental data for a variety of adsorption systems has provided strong support for this point of view [3].

In this paper we focus on features not discussed earlier [6]: the range of the average density of the adsorbate, the order of the transition, the orientational degeneracy of the ground state, the isosteric heat of adsorption of the system, and the effect of the vertical cell dimension. In the following section, we discuss the methods used in this sim-

ulation study. Section II introduces briefly the method. Section III reports the results and compares them with recent experiments from our group. Section IV summarizes these results, draws conclusions and comments on strategies for future research in this area.

## II. METHOD

We study the adsorption of Xe on the tenfold surface of the decagonal  $\text{Al}_7\text{Ni}_{10}\text{C}_{017}$  quasicrystal (QC) using the grand canonical Monte Carlo simulation method (GCMC) [10,11]. Since this technique is widely used and we have described our method in detail previously [7,12], only a brief description is given here. At constant volume,  $V$ , and temperature,  $T$ , the GCMC method explores the configurational phase space, using the familiar Metropolis algorithm, and finds the equilibrium number of adsorbed atoms,  $N$ , as a function of the chemical potential,  $\mu$ , of Xe.  $\mu$  is related to the pressure of the coexisting gas, which is taken to be ideal. We also determine density profiles,  $\rho(x,y)$ , and adsorption isotherms,  $N$ , as a function of the pressure,  $P(T; \mu)$ . For each data point in an isotherm, 18 million GCMC steps (each step being an attempted creation, deletion, or displacement of an atom) are performed to reach nominal equilibrium and 27 million steps are performed in the subsequent data-gathering phase. Displacements, creations, and destructions of atoms are executed with probabilities equal to 0.2, 0.4, and 0.4, respectively [12].

The interaction potentials used in the calculations are based on the 12-6 Lennard-Jones (LJ) functional form of pair interaction. The construction of the interactions is described in detail in references [6,13-15]. Using these potentials, we perform simulations in a tetragonal cell. The height of the cell, along the  $z$  (surface-normal) direction, is chosen to be 10 nm (long enough to contain 20 layers of Xe). At the top of the cell, a hard-wall reflective potential is simulated to confine the vapor. The base of the cell has dimensions of  $5.12 \times 5.12$  nm<sup>2</sup> and periodic boundary conditions are employed along the  $x$  and  $y$  directions. These periodic boundary conditions render the surface effectively infinite; we use a relatively large cutoff

(5<sub>gg</sub>) to minimize long range interaction corrections.

Figure 1 (a) shows the function  $V_{\text{min}}(\mathbf{x};y)$ , which is calculated by minimizing the adsorption potential along the  $z$  direction at every value of the planar coordinates  $(\mathbf{x};y)$ :

$$V_{\text{min}}(\mathbf{x};y) = \min_z (V(\mathbf{x};y;z))_{\text{along } z} \quad (1)$$

Such a figure reveals the fivefold rotational symmetry of the substrate. Dark regions in the figure correspond to the most attractive regions on the substrate. By choosing appropriate sets of five dark spots, we can identify pentagons, which correspond to the inflated tile of a pentagonal Penrose tiling. The sizes of the pentagons follow the incommensurate property of the QC structure.

### III. RESULTS AND DISCUSSION

A layer-by-layer growth mode for Xe on this QC surface was observed and reported earlier [6]. Figure 1 (b) shows a particular isotherm at  $T = 77\text{K}$  with the formation of the first and second layers.

Density of the adsorbate. A detailed study of the density profiles of the isotherms shows that the range of the density of the monolayer is considerably larger than that of the bilayer. For example, at  $77\text{K}$ , the average density of the monolayer increases from  $4.09 \text{ atom/s/nm}^2$  at its formation to  $5.74 \text{ atom/s/nm}^2$  at its completion (a 40% increase) whereas for the bilayer, it increases from  $10.84 \text{ atom/s/nm}^2$  at its formation to  $10.98 \text{ atom/s/nm}^2$  at its completion (less than 2% increase). The density increase of the monolayer is several times larger than that observed experimentally for Xe on  $\text{Ag}(111)$ , a much flatter substrate [16]. The difference is due to the much larger lateral variation in adsorption energy experienced by the Xe on the QC surface. The magnitude of this variation is apparently much smaller for the second layer.

Order of the transition. An interesting phenomenon that we have found in this system is the continuous rearrangement of Xe atoms in the monolayer, which leads to the ordering transition from fivefold to sixfold. Such reordering appears to be continuous in the evolution of the location of the first peak in the pair correlation function shown in Figure 2 (b) of reference [6]. However, there are some peculiarities that must be explained in detail.

To better characterize the evolution of the adsorption process we define a reduced chemical potential  $\mu^*$ , as:

$$\mu^* = \frac{\mu - \mu_1}{\mu_2 - \mu_1}; \quad (2)$$

where  $\mu_1$  and  $\mu_2$  are the chemical potentials at the onset of the first and second layer formation, respectively. In addition, we introduce an order parameter,  $P_{5-6}$ , which is defined as the probability of fivefold defects:

$$P_{5-6} = \frac{N_5}{N_5 + N_6}; \quad (3)$$

where  $N_5$  and  $N_6$  are the number of atoms having 2D coordination number equal to 5 and 6, respectively. The

2D coordination number is the number of neighboring atoms within a cutoff radius of  $1.366 \times 0.44 \text{ nm} = 0.601 \text{ nm}$  ( $1.366 = \cos(\pi/6) + 1 = 2$  is the average of the 1st NN and the 2nd NN in a triangular lattice);  $0.44 \text{ nm}$  is taken from the 1st NN distance of Xe at  $77\text{K}$  (note that this distance does not change appreciably between  $0.440 \text{ nm}$  at  $77\text{K}$  and  $0.443 \text{ nm}$  at  $140\text{K}$  [6]).

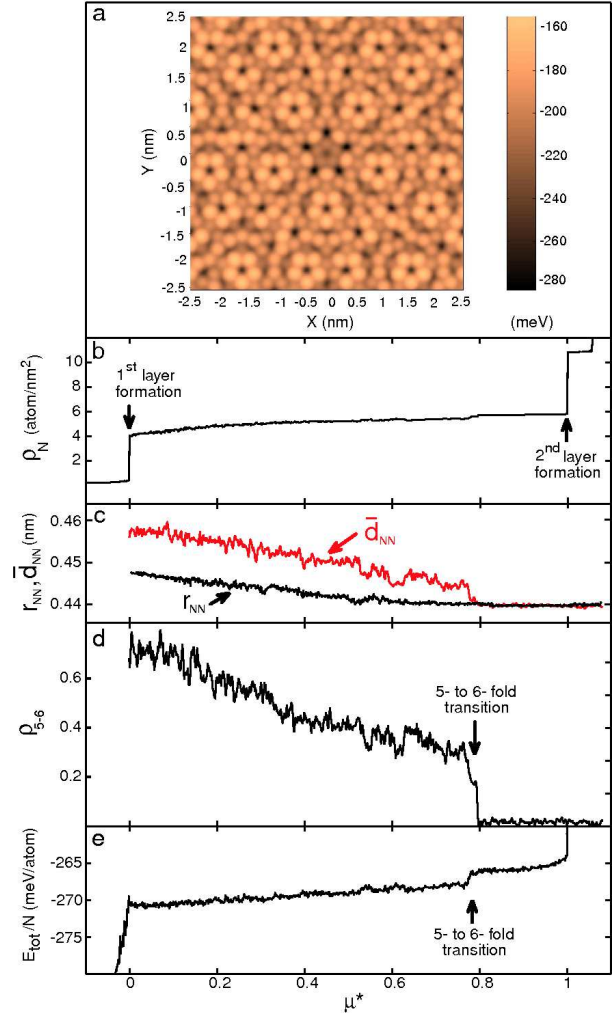


FIG. 1. (color online). (a) Minimum potential energy surface,  $V_{\text{min}}(\mathbf{x};y)$ , for Xe on a  $5.12 \times 5.12 \text{ nm}^2$  section of QC. The scale at the right shows the energy scale, which ranges from  $-280$  to  $-160 \text{ meV}$ . (b) Adsorption isotherm,  $\rho_N$ , versus the reduced chemical potential,  $\mu^*$ , at  $T = 77\text{K}$ . (c) Nearest neighbor distance defined from the pair correlation function,  $r_{\text{NN}}$ , (black line), and average spacing between neighbors at equilibrium,  $d_{\text{NN}}$ , (red line). (d) Order parameter  $P_{5-6}$  (probability of fivefold defects, defined in Eq. 3) versus the reduced chemical potential,  $\mu^*$ , at  $T = 77\text{K}$ . (e) Total energy per atom at  $T = 77\text{K}$ . The transition, which is defined as the point in  $\mu^*$  above which the order parameter remains nearly constant, occurs at  $\mu_{\text{tr}}^* \approx 0.8$ . The discontinuity in  $E_{\text{tot}}/N$  around  $\mu_{\text{tr}}^* \approx 0.8$  indicates a latent heat of the transition. The order parameter  $P_{5-6}$  after the transition is  $0.017$ .

Figure 1 (d) shows a plot of order parameter  $P_{5-6}$  versus the reduced chemical potential for  $T = 77\text{K}$ . It starts from

0.8 at the first layer formation and gradually decreases. It drops and remains at a nearly constant value of 0.017 for  $\mu_{tr}^* > 0.8$ , where  $\mu_{tr}^*$  is a transition reduced chemical potential at 77K. Figure 1(e) shows the total energy per atom,  $E_{tot} = N \cdot \mu_{tr}^*$ . At the transition point  $\mu_{tr}^*$ , the energy per atom has a little step indicating a latent heat of the transition. The discontinuity of the order parameter  $\rho_{5-6}$  and the presence of latent heat indicate that the transition is first-order.

In spite of this evidence for a first-order transition, the nearest neighbor distance, labeled  $r_{NN}$  in Figure 1(c), appears to change continuously. This nearest neighbor distance, also reported in our earlier paper [6], was defined as the location of the first peak in the pair correlation function because the latter property is more directly comparable to diffraction measurements. Here we have also calculated the average spacing between neighbors,  $d_{NN}$ , which is a thermodynamically meaningful quantity (related to the density). This has a small discontinuity at the transition, providing additional evidence for the first-order character of the transition. Both quantities,  $r_{NN}$  and  $d_{NN}$ , are shown in Figure 1(c). The NN Xe-Xe distance  $r_{NN}$  decreases continuously as  $P$  increases, starting from 0.45 nm and saturating at 0.44 nm. The Xe-Xe distance reaches saturation value before the appearance of the second layer; therefore, the transition is complete within the first layer. We note that a similar decrease in NN distance was measured for Xe/Ag(111), but in that case, the NN spacing did not saturate before the onset of the second layer adsorption [16,17].

Defects are present at all temperatures that we have simulated (in the interval 20K to 286K). The probability of defects increases with temperature, implying that their origin is entropic, as is the case for a periodic crystal. Figure 2-(right axis) shows that the defect probability increases as  $T$  increases, while Figure 2-(left axis) shows the trend of the transition point in function of  $T$ . At low temperatures, the sixfold ordering occurs earlier (at lower  $\mu_{tr}^*$ ) as the temperature is increased from 40K to 70K. This trend is expected because the ordering effect imposed by the substrate corrugation becomes relatively smaller as the temperature increases. However, this trend is not observed in the higher temperature region (from 70K to 140K). In fact, at higher temperatures the transition point shifts again to higher  $\mu_{tr}^*$ . This is most likely due to the monolayer becoming less two-dimensional, allowing more structural freedom of the Xe atoms and thus decreasing the effect of the repulsive Xe-Xe interaction that would stabilize the sixfold structure. Transitions having critical  $\mu_{tr}^* > 1$  indicate that the onset of second-layer adsorption occurs earlier than the transition to the sixfold structure. When the second layer adsorbs at  $T > 130K$ , the density of the monolayer increases by a few percent, thereby increasing the effect of the repulsive interactions and driving the vefold to sixfold transition.

The fact that the structural transition for Xe occurs entirely within the first layer suggests that atoms in subsequent layers are arranged in a triangular lattice, which is indeed the case [6]. Furthermore, this finding suggests

that the effect of the corrugation of the adsorption potential on the structure of further layers is quite small. The large corrugation experienced by the first layer combined with the structural mismatch of the substrate and the Xe(111) plane causes more variation in the local structures of the atoms in the first layer. This explains why the first-layer step in the isotherm is broader than the second-layer step, and why the density variation during the evolution of the bilayer is smaller, as pointed out earlier. When the second layer begins to form, our simulations indicate a slightly (about 0.01 nm) larger NN spacing for the second layer than for the first layer. A similar coexistence of two lattice spacings was also found in calculations for Xe/Ag(111) [19] but was not observed experimentally for that system or for this one.

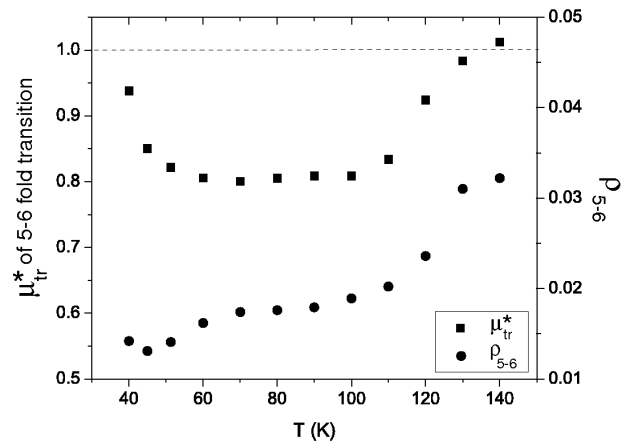


FIG. 2. Values of  $\mu_{tr}^*$  for the vefold to sixfold transition points from 40K to 140K (left axis). Transition points at  $\mu_{tr}^* > 1$  indicate that a transfer of atoms from the second layer to the first layer is required to complete the transition. Also shown is the defect probability as a function of  $T$  after the transition occurs (right axis), indicating an increase in defect probability with  $T$ .

The observed transition from vefold to sixfold order within the first layer can be viewed as a commensurate-incommensurate transition (CII), since at the lower coverage, the layer is commensurate with the substrate symmetry and aperiodic, while at higher coverage, it is incommensurate with the substrate. Such transitions within the first layer have been observed before for adsorbed gases, perhaps most notably for Kr on graphite [20]. There, as here for Xe, the Kr forms a commensurate structure at low coverage, which is compressed into an incommensurate structure at higher coverage. The opposite occurs for Xe on graphite, which is incommensurate at low coverage and commensurate at high coverage [21]. Such commensurate-incommensurate transitions have been studied theoretically in many ways, but perhaps most simply as a harmonic system (balls and springs) having a natural spacing that experiences a force field having a different spacing [22]. Such a transition has been found to be first-order for strongly corrugated potentials (in 1D) but continuous for

more weakly corrugated potentials [23]. The transition observed in our quasicrystal surface suggests that system is within the regime of "strong" corrugation, which was not the case of Kr over graphite [20]. In fact, for the latter system, both commensurate and incommensurate structures have sixfold symmetry. A more relevant comparison may be the transition of Xe on Pt(111), from a rectangular symmetry incommensurate phase to a hexagonal symmetry commensurate one, although in that case, the low-temperature phase was incommensurate. That transition was also found to be continuous [24]. Therefore, while our simulations indicate that Xe on AlNiCo undergoes a CII, as observed for other adsorbed gases, the observation of a first-order CII is new, to our knowledge, and likely arises from the large corrugation. Simulations with other noble gases, possessing different values of  $\epsilon_{gg}$  and  $\epsilon_{gg}$ , would give insight into the origin and location of the transition [18]. Simulations carried out with decreasing pressure in this region show some hysteresis. While hysteresis is often interpreted as evidence of a first-order transition, this is not necessarily the rule. For example previous calculations have exhibited hysteretic behavior within a monolayer on a very heterogeneous surface, where no transition occurs [25,26].

**Oriental degeneracy of the ground state.** In our earlier paper, it was described that after the ordering transition is complete, the resulting sixfold structure is aligned parallel to one of the sides of the pentagons in the  $V_m$  map of the adsorption potential (there are five possible orientations). In the experiments, all five orientations are observed, due to the presence of all possible alignments of hexagons along five sides of a pentagon in the QC sample within the width of the electrons beam ( $\approx 0.25$  nm). In an ideal infinite GCMC framework the ground state of the system would be degenerate and all five orientations would have the same energy and be equally probable. However, the square periodic boundary conditions of our GCMC break this orientational degeneracy, causing some orientations to become more likely to appear.

To find all the possible orientations, we performed simulations with a cell having free boundary conditions. The cell is a  $5.12 \times 5.12$  nm<sup>2</sup> quasicrystal surface surrounded by vacuum. Figure 3(a) shows the  $V_m$  map of the adsorption potential. Thirty simulations at 77K are performed with this cell. The isotherms from these runs are plotted in Figure 3(b). Only the first layer is shown, and the finite size of the surface makes the growth of the first layer continuous. The density profiles  $\rho(x;y)$  of all the simulations are analyzed at point  $p^2$  of Figure 3(b). In this cell, all five orientations of hexagons are observed with equal frequency indicating the orientational degeneracy of the ground state. To represent the five orientations, density profiles of five calculations (c, d, e, f, and g) are shown in Figures 3(c) to 3(g) with their FT plotted on the side. Figure 3(h) presents a schematic depiction of which orientations of hexagons are exemplified in each simulation.

Figures 4(a) and 4(b) illustrate the effect of pentagonal defects on the orientation of hexagons at point  $p^2$  of Figure 3(b). In most of the density profiles correspond-

ing to this coverage, we find the behavior shown in Figure 4(a). Here, the effect of the pentagonal defect, which is the center of a dislocation in the hexagonal structure, is to rotate the orientation of the hexagons above the pentagon by  $2\pi/5 = 72^\circ$  with respect to the hexagons below the pentagon. The possible rotations are  $n \times 72^\circ$ , where  $n = 1, 2, 3, 4$ , or 5. The rotation by  $72^\circ$  is usually mediated by more than one equivalent pentagon, as is shown in Figure 4(b) (note the "up" pentagon at the middle-bottom part and the "down" pentagon near the middle-top part of the figure). The "up" pentagon (with one vertex on the top) is equivalent with the "down" pentagon (with one vertex on the bottom) since they have five orientationally equivalent sides). These pentagonal defects are induced by the fivefold symmetry of the substrate, and their concentration decreases in the subsequent layers.

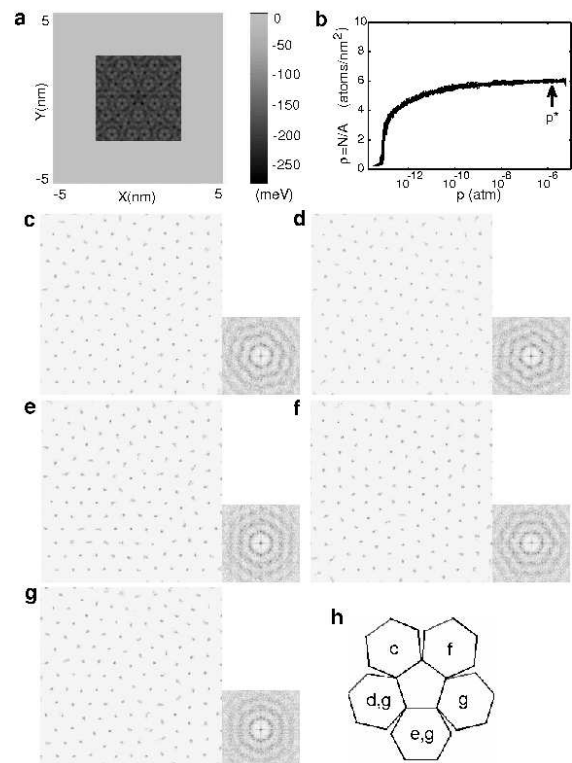


FIG. 3. (a) Minimum potential energy surface of the adsorption potential with free boundary conditions. (b) Adsorption isotherms of the first layer from a set of 30 simulations at 77K using the free cell described in the paper. Five density profiles and FTs at point  $p^2$  of (b) are shown in (c) to (g), representing all possible orientations of hexagonal domains. (h) Schematic diagram illustrating the correspondence between the orientations of the hexagonal domains observed in the density profiles (c) to (g).

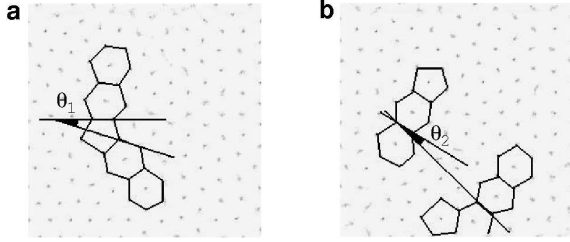


FIG. 4. Pentagonal defects rotate the orientation of hexagons by (a)  $\theta_1 = 24^\circ$  and (b)  $\theta_2 = 12^\circ$ .

Isosteric heat of adsorption. Figure 5 shows a  $P$ - $T$  diagram for three different coverages constructed from the isotherms in the range  $40\text{K} < T < 110\text{K}$ . In the GCMC simulations the layers grow step-wise; at  $70\text{K}$  the first step occurs between coverage 0.06 and 0.7, the second step occurs between coverage 1.0 and 1.9, and the third step occurs between coverage 1.9 and 2.8 (unit is in fractions of monolayer). Figure 5 shows the  $T$ ,  $P$  location of these steps, denoted  $\backslash\text{cov } 0.5$ ",  $\backslash\text{cov } 1.5$ ", and  $\backslash\text{cov } 2.5$ " for the first, second, and third steps, respectively. The isosteric heat of adsorption per atom at these steps can be calculated from this  $P$ - $T$  diagram as follows [16]:

$$q_{\text{st}} = k_B \frac{d(\ln P)}{d(1/T)_n} : \quad (4)$$

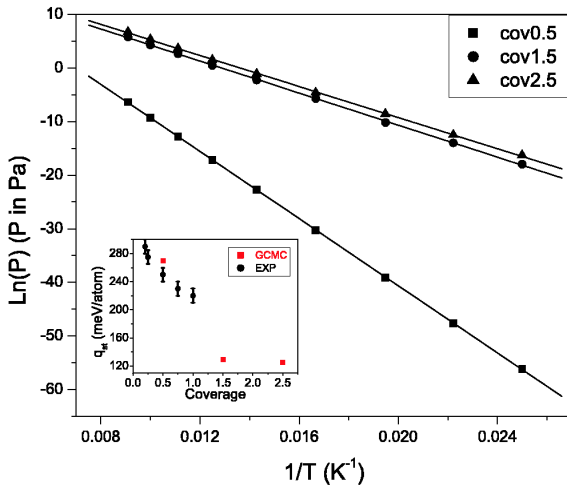


FIG. 5. (color online). Locations in  $P$ ,  $T$  of the vertical risers in the isotherms corresponding to the first (square), second (circle), and third (triangle) layer formation. The heats of adsorptions,  $q_{\text{st}}$ , are 270, 129, and 125 meV/atom respectively, calculated as described in the text. The inset figure shows  $q_{\text{st}}$  obtained from the simulations as well as from the experiments.

The inset of Figure 5 summarizes the values of  $q_{\text{st}}$  obtained from simulations and experiments. The agreement between experiment and the simulations for the half monolayer heat of adsorption is good. The values obtained in the simulation for the 1.5 and 2.5 layer heats are about 20% lower than the bulk value of 165 meV [27]. The lower values suggest that bulk formation should be preferred at coverages above one layer. However, layer-by-layer growth

is observed at all  $T$  for at least the first few layers in these simulations. We therefore believe that the low heats of adsorption arise from slight inaccuracies in the Xe-Xe LJ parameters used in this calculation, as the heats of adsorption are very sensitive to the gas parameters.

Effect of the vertical dimension. In our earlier study only 2 steps, corresponding to the first and second layer adsorption, were apparent in the isotherms [6]. Further simulations indicate that when the cell is extended in the vertical direction, additional steps are observed. Therefore the number of observable steps is related to the size of the cell. Nevertheless, layering is clearly evident in the  $(z)$  profile, and the main features of the film growth are not altered. The average interlayer distance is calculated to be about 0.37 nm, compared to 0.358 nm for the interlayer distance in the  $\langle 111 \rangle$  direction of bulk Xe [28]. Our simulations of multilayers show variable adsorption as the simulation cell is expanded in the direction perpendicular to the surface. This is a result of sensitivity to perturbations (here, cell size) close to the bulk chemical potential, where the wetting film's compressibility diverges. This dependence has been seen previously in large scale simulations. See e.g. Figure 3 of reference [29]. The analog of this effect in real experiments is capillary condensation at pressures just below saturated vapor pressure ( $\text{svp}$ ), the difference varying as the inverse pore radius.

#### IV. CONCLUSIONS

One of the main motivations for the study of Xe on the QC surface was to elucidate which adsorption phenomena are due to the QC structure of the substrate, as opposed to chemical interactions between the adatoms and the substrate. We have discovered a system that is rich with interesting phenomena, some of which are common to other physisorption systems and some that are different. The features that have been observed include layer-by-layer growth at low temperatures, complete wetting above the 3D triple point, a first-order phase transition from a "commensurate" structure to an incommensurate hexagonal close-packed structure within the monolayer regime, substrate-induced alignment of the incommensurate film, and an increase in defect probability with temperature. Above a monolayer, the structure continues to grow in hexagonal close-packed layers [6]. The features that are different are specific to the  $\sqrt{3} \times \sqrt{3}$  symmetry of the substrate, and include a  $\sqrt{3}$ -fold commensurate structure and a  $\sqrt{3}$ -fold to sixfold structural transition. We have observed some other phenomena for which we are unaware of previous reports, including the U-shaped curve of commensurate-incommensurate transition chemical potential  $\mu_{\text{tr}}^?$  versus temperature and orientational domain boundaries generated by pentagonal defects. It would be interesting to investigate how these features are affected by different potential parameters, and further investigations for Ne, Ar and Kr adsorption on this surface are in progress [18].

The agreement between the simulations reported here and the corresponding experimental studies by our group are very good, perhaps better than might be expected, although good correspondence was already observed earlier in calculations of the low-coverage properties of this system [14]. The main points of comparison are the nature of the  $\ln$  growth, the submonolayer isosteric heat of adsorption, and the structure of the  $\ln$  above one monolayer. The high level of agreement for these features indicates that LJ potentials provide a good description of the interactions in this system, at least those pertaining to the main features of the  $\ln$  growth. Despite this good agreement, one might question the use of LJ potentials in light of experimental observations that Xe atoms on metal surfaces have a preference for low-coordination sites [30]. That preference is believed to originate from a screening response of the metal to the adsorbed Xe [31]. At this time, there are no experimental measurements of adsorption sites for Xe on QC surfaces, but the good agreement found here for  $\ln$  growth suggests that any such screening interactions have a negligible effect on the global adsorption behavior, which is also the case for metal surfaces.

It would be very useful to have experimental measurements that would elucidate the structure of the monolayer Xe  $\ln$ . LEED experiments sample the outer several layers of the sample, making it difficult to differentiate between the Xe structure and the substrate structure if they are the same, as indicated by these simulations. Low-temperature STM experiments on this system have thus far been inconclusive because of the difficulty of establishing a tunneling current through the Xe to the weakly-conducting QC substrate. An ideal probe of the monolayer structure would be He-atom diffraction, which has been used for similar measurements of metal  $\ln$ s on QC surfaces [32], and such measurements are planned.

#### V. ACKNOWLEDGMENTS

We gratefully acknowledge useful interactions with Raluca A. Trasca, Chris Henley, David Rabson, Aleksey Kolmogorov, Katarina Pussi, Hsin-Li, and L.W. Burch. We acknowledge the San Diego Supercomputer Center for computing time under Proposal Number M5S060002. This material is based upon work supported by the National Science Foundation under Grant Nos. 0208520 and 0505160. We are grateful to critical comments of the referees of this paper.

- 
- [1] J. G. Dash, M. Schick, and O. E. Vilches, *Surf. Sci.* 300, 405-414 (1994).  
 [2] D. Nicholson and N. G. Parsonage, *Computer simulation and the statistical mechanics of adsorption*. 1982, London: Academic Press.  
 [3] L. W. Burch, M. W. Cole, and E. Zaremba, *Physical Adsorption*. 1997: Oxford U. P.  
 [4] L. M. Sander and J. H. Austman *Phys. Rev. B* 29, 2171-2174 (1984).

- [5] D. K. Fairbrother, W. F. Saam, and L. M. Sander, *Phys. Rev. B* 26, 179-183 (1982).  
 [6] S. Curtarolo, W. Setyawan, N. Ferralis, R. D. Diehl, and M. W. Cole, *Phys. Rev. Lett.* 95, 136104 (2005).  
 [7] R. D. Diehl, N. Ferralis, K. Pussi, M. W. Cole, W. Setyawan, and S. Curtarolo, *Phil. Mag.* 86, 863-868 (2006).  
 [8] I. R. Fisher, M. J. Kramer, Z. Islam, A. R. Ross, A. Kracher, T. W. Heener, M. J. Sailer, A. I. Goldman, and P. C. Canfield, *Phil. Mag. B* 79, 425-434 (1999).  
 [9] V. Fomene and P. A. Thiel, *J. Phys. D: Appl. Phys.* 38, R83-R106 (2005).  
 [10] D. Frenkel and B. Smith, *Understanding Molecular Simulations: From Algorithms to Application*, 2002, New York: Academic.  
 [11] M. P. Allen and D. J. Tildesley, *Computer Simulation of Liquids*, 1987, Oxford: Oxford U. P.  
 [12] M. J. Bojan, G. Stan, S. Curtarolo, W. A. Steele, and M. W. Cole, *Phys. Rev. E* 59, 864-873 (1999).  
 [13] N. Ferralis, K. Pussi, E. J. Cox, M. Gierer, J. Ledieu, I. R. Fisher, C. J. Jenks, M. Lindroos, R. M. McGrath, and R. D. Diehl, *Phys. Rev. B* 69, 153404 (2004).  
 [14] R. A. Trasca, N. Ferralis, R. D. Diehl, and M. W. Cole, *J. Phys.: Condens. Matter* 16, S2911-S2921 (2004).  
 [15] Reference [3]: p. 67.  
 [16] J. Unguris, L. W. Burch, E. R. Moog and M. B. Webb, *Surf. Sci.* 87, 415-436 (1979).  
 [17] P. Dai, T. Angot, S. N. Ehrlich, S.-K. Wang, and H. Taub, *Phys. Rev. Lett.* 72, 685 (1994).  
 [18] W. Setyawan, N. Ferralis, R. D. Diehl, M. W. Cole, and S. Curtarolo, in preparation (2006).  
 [19] L. W. Burch, J. Unguris, and M. B. Webb, *Surf. Sci.* 87, 437-456 (1979).  
 [20] M. D. Chinn and S. C. Fain, Jr., *Phys. Rev. Lett.* 39, 146 (1977).  
 [21] P. S. Schabes-Retchkin and J. A. Venables, *Surf. Sci.* 105, 536-564 (1981).  
 [22] F. C. Frank and J. H. Van der Merwe, *Proc. Roy. Soc. London, Ser. A* 198, 205 and 216 (1949) and 200, 125 (1949).  
 [23] S. C. Ying, *Phys. Rev. B* 3, 4160 (1971).  
 [24] K. Kem, R. David, P. Zeppenfeld, R. Palm er, and G. Comsa, *Solid State Comm.* 62, 391-394 (1987).  
 [25] L. E. Cascarini de Torre and E. J. Bottani, *Langmuir* 13 3499 (1997).  
 [26] M. C. Calbi, S. M. Gatica, M. J. Bojan, M. W. Cole, *J. Chem. Phys.* 115, 9975 (2001).  
 [27] N. Ferralis, R. D. Diehl, K. Pussi, M. Lindroos, I. Fisher, and C. J. Jenks, *Phys. Rev. B* 69, 075410 (2004).  
 [28] P. Korpiun and E. Luscher, *Thermal and elastic properties at low pressure*, in *Rare Gas Solids*, ed. M. L. Klein and J. A. Venables, Vol. II. 1977, New York: Academic Press.  
 [29] S. Curtarolo, G. Stan, M. J. Bojan, M. W. Cole, and W. A. Steele, *Phys. Rev. E* 61, 1670-1675 (2000).  
 [30] R. D. Diehl, T. Seyller, M. Caragiu, G. S. Leathersman, N. Ferralis, P. Kaukasova, M. Lindroos and K. Pussi, *J. Phys. Cond. Mat.* 16, S2839 - S2862 (2004)  
 [31] J. L. F. da Silva, C. Stamp, and M. Scheer, *Phys. Rev. Lett.* 90, 066104 (2004); *Phys. Rev. B* 72, 075424 (2005).  
 [32] K. J. Franke, H. R. Sharma, W. Theis, P. Gilke, P. Ebert, and K. H. Rieder, *Phys. Rev. Lett.* 89, 156104 (2002).